Solar Energy 164 (2018) 47–57

Contents lists available at ScienceDirect

Solar Energy

journal homepage: www.elsevier.com/locate/solener

Containment materials for liquid tin at 1350 °C as a heat transfer fluid for high temperature concentrated solar power

Yunshu Zhang[a], Ye Cai[a], SungHwan Hwang[c], Gregory Wilk[b], Freddy DeAngelis[b], Asegun Henry[a,b,*], Kenneth H. Sandhage[a,c,*]

[a] School of Materials Science and Engineering, Georgia Institute of Technology, Atlanta, GA 30332, United States
[b] George W. Woodruff School of Mechanical Engineering, Georgia Institute of Technology, Atlanta, GA 30332, United States
[c] School of Materials Engineering, Purdue University, West Lafayette, IN 47905, United States

ARTICLE INFO

Keywords:
Containment materials
Liquid tin heat transfer fluid
High temperature (1350 °C)
Concentrated solar power

ABSTRACT

One pathway for reducing the cost of concentrated solar power (CSP) is to increase the system efficiency by operating a heat engine with a higher hot side (inlet) temperature. If a turbine is used, then a system utilizing a combined cycle could potentially reach upwards of ~60% efficiency, provided that the turbine could be operated with an inlet temperature > 1300 °C. Such high temperatures place severe limits on heat transfer fluids; that is, such fluids would need to remain chemically stable, and be compatible with containment materials, at such extreme temperatures. One potential class of such fluids are liquid metals, such as molten tin. While possessing low melting and high boiling points (232 °C and 2600 °C, respectively) for a high operational range, molten tin also tends to be highly corrosive towards common structural metal alloys used as components for the containment and controlled flow of liquids (*i.e.*, for pipes, tanks, valves, pumps, etc.). Thus, it would be useful to identify materials that are compatible with molten tin at ≥1300 °C. The purpose of this paper is to evaluate three candidate high-temperature materials, possessing a range of thermal conductivities, for the containment of molten tin: graphite (C), silicon carbide (SiC), and mullite ($Al_6Si_2O_{13}$). The corrosion and penetration of these materials by molten Sn or doped Sn liquids at 1350 °C for 100 h were evaluated via local electron microscopic analyses and global weight change measurements. Under appropriate conditions, all three of these materials exhibited minimal to no reaction with tin-based liquids at 1350 °C and were not penetrated by these liquids at this temperature. This work indicates that graphite, silicon carbide, and/or mullite can serve as effective containment materials for the use of tin-based liquids as heat transfer fluids operating at 1350 °C in CSP plants.

1. Introduction

The cost of concentrated solar power (CSP) with thermal energy storage (TES) has been estimated to be 13.5–20 ¢/kWh$_e$ (Hernandez-Moro and Martinez-Duart, 2013; Margolis et al., 2012; Kolb et al., 2011). While current flat plate photovoltaic solar technologies have a lower levelized cost of electricity (LCOE), their output is not dispatchable. If electrical batteries are added to such photovoltaic systems to provide dispatchability, then the combined cost can be greater than for CSP/TES systems (Dunn et al., 2011; Rastler, 2010). While CSP/TES systems can be cost-effective options for dispatchable solar power, direct competition with fossil fuel-based power generation requires that the CSP/TES LCOE (*i.e.*, for state-of-the-art power tower configurations with molten salt TES) be further reduced by > 50% (U.S. Energy Administration Information, 2015; Kolb et al., 2011).

The LCOE for CSP may be significantly reduced by increasing the overall system efficiency via use of more efficient heat engines. However, current turbomachinery-based heat engines already operate near their thermodynamic limits (Henry and Prasher, 2014). Thus, one of the only strategies for major increases in turbine efficiency would be to operate with a much higher turbine inlet temperature (TIT) (Henry and Prasher, 2014). It should be noted that several prior system analyses have indicated that operating at higher temperatures is of critical importance for realizing major LCOE reductions (Margolis et al., 2012; Mehos et al., 2016). However, depending upon the peak temperature used, there could be other efficiency trade-offs in the optics, receiver, or storage. Nonetheless, it is worthwhile to identify potential materials that could allow for a wider range of peak CSP operational temperatures.

The highest-efficiency, long-life heat engine systems utilize combined

* Corresponding authors at: George W. Woodruff School of Mechanical Engineering, Georgia Institute of Technology, Atlanta, GA 30332, United States (A. Henry). School of Materials Engineering, Purdue University, West Lafayette, IN 47907, United States (K.H. Sandhage).
E-mail addresses: ase@gatech.edu (A. Henry), sandhage@purdue.edu (K.H. Sandhage).

https://doi.org/10.1016/j.solener.2018.01.085
Received 17 May 2017; Received in revised form 5 December 2017; Accepted 29 January 2018
Available online 14 March 2018
0038-092X/

cycles and would require TITs in the range of 1300–1500 °C to achieve efficiencies up to ~60% (Huck et al., 2016; Brooks, 2000). An increase in heat-to-electricity conversion efficiency from 35 to 40% (current heat engines) to 60% corresponds to a 50–71% increase in relative efficiency. If all other plant costs remained fixed, then such an enhancement in relative efficiency would result in a cost reduction of 33–42%, which would be a major step towards parity with fossil fuel-derived electricity. Hence, approaches enabling the operation of CSP systems at such high temperatures should be considered.

A variety of liquids (*e.g.*, molten salts, glasses, metals) have been considered as high-temperature heat transfer agents (Elkin et al., 2014; Pacio and Wetzel, 2013; Forsberg et al., 2006; Misra and Whittenberger, 1987). Liquid metals can be particularly attractive, due to their relatively high values of thermal conductivity (usually ~10–100 $W\,m^{-1}\,K^{-1}$), low values of viscosity (typically ~1 cP), and (for certain metals) relatively high ranges of thermal stability (*i.e.*, low melting points and high boiling points) (Pacio and Wetzel, 2013; Sobolev, 2012, 2010; Ghoshal et al., 2005; Regel et al., 1971). When considering the parasitic loads associated with pumping various heat transfer liquids at the MW scale, these attractive characteristics of liquid metals can lead to notable system level performance advantages and, ultimately, cost benefits.

The use of liquid metals as heat transfer fluids has been recently reviewed for nuclear and CSP systems (Pacio and Wetzel, 2013; Pacio et al., 2014). Among potential liquid metals for heat transfer are group 13 and 14 elements, such as Al, Sn, and Pb. These metals have low melting points (660 °C, 232 °C, and 328 °C, respectively) and high boiling points (2518 °C, 2600 °C, and 1746 °C, respectively) for wide operational temperature ranges (Barin, 1995). Molten Pb is unattractive from a health and environmental perspective (Goyer, 1990), and molten Sn and Al are quite corrosive towards Ni-based and Fe-based alloys (and numerous other metal alloys) at elevated temperatures (Emmerich and Schroer, 2017; Heinzel et al., 2017; Dybkov, 1990; Reed, 1954). Because molten aluminum has a higher affinity for oxygen, nitrogen, and carbon than does molten tin (Pietzka and Schuster, 1997; Barin, 1995; Oden and Gokcen, 1993), molten tin is expected to be generally less reactive than molten aluminum with refractory oxides, nitrides, carbides, and carbon. Nonetheless, experimental evaluation of the chemical compatibility of molten Sn with potential high-temperature refractory containment materials at > 1300 °C is needed.

The aims of this paper are therefore: (i) to assess the relative thermochemical and thermophysical properties of three candidate commercially-available refractory materials for the containment of tin-based liquids at 1350 °C: graphite (C), silicon carbide (SiC), and mullite ($Al_6Si_2O_{13}$); (ii) to evaluate the resistances of graphite, silicon carbide, and mullite to chemical interaction with, and penetration by, various grades (purities) of molten tin at 1350 °C; and (iii) to identify conditions under which such chemical interaction/penetration can be avoided or reduced.

2. Thermochemical and thermophysical properties of graphite, silicon carbide, and mullite at 1350 °C

Graphite, silicon carbide, and mullite were selected for evaluation as candidate high-temperature containment materials for tin-based liquids at 1350 °C (the temperature selected for experimental work in this paper) after considering the following characteristics:

- thermal stability
- chemical compatibility with molten tin
- wetting and penetration by molten tin
- resistance to oxidation or reduction
- thermal conductivity
- thermal expansion
- high-temperature stiffness and creep resistance
- commercial availability and relative cost

Regarding thermal stability, graphite undergoes sublimation at 1 atm above 3600 °C (Joseph et al., 2002; Barin, 1995; Leider et al., 1973). Silicon carbide melts incongruently to form solid carbon and a silicon-rich liquid at ≥2540 °C (Kleykamp and Schumacher, 1993; Olesinski and Abbaschian, 1984b; Scace and Slack, 1959). Mullite is also reported to melt incongruently, to yield a mixture of solid alumina and a silica-alumina liquid, at 1890 °C (Klug et al., 1987; Horibe and Kuwabara, 1967).

Regarding chemical compatibility with liquid tin, graphite is not reported to form a stable carbide by reaction with tin at ambient pressure (Pietzka and Schuster, 1997) and the solubility of graphite in pure liquid tin is low. Extrapolation of the data of Oden and Gokcen (1993) from 1550 °C–2300 °C down to 1350 °C yields a carbon solubility in liquid tin (99.999% purity) of only 0.34 ppm at 1350 °C. The Si-C-Sn ternary phase diagram, and the solubility of SiC in liquid Sn at 1350 °C, do not appear to have been evaluated. The chemical interaction of mullite ($Al_6Si_2O_{13}$) with liquid tin at 1350 °C also does not appear to have been reported. As for other oxide/liquid systems (Kumar et al., 1999; Sandhage and Yurek, 1991, 1990b, 1990a, 1988), the incongruent reaction of mullite ($Al_6Si_2O_{13}$) with pure liquid tin at 1350 °C via the following reactions may be considered:

$$2Sn(l) + Al_6Si_2O_{13}(s) = 2SnO_2(s) + 2\{Si\} + 3Al_2O_3(s) \quad (1)$$

$$4.5Sn(l) + Al_6Si_2O_{13}(s) = 4.5SnO_2(s) + 6\{Al\} + 2SiO_2(s) \quad (2)$$

where {Si} and {Al} refer to silicon and aluminum dissolved in molten tin, respectively. However, thermodynamic analyses (see Supplemental Information) indicate that the extent of decomposition of mullite by incongruent reduction reactions (1) and (2) at 1350 °C should be negligible. While it is expected that graphite, silicon carbide, and mullite should exhibit good chemical compatibility with high-purity liquid tin at 1350 °C, the chemical compatibility of these potential containment materials with lower purity, commercially-available liquid tin is unclear.

Regarding liquid tin wetting and penetration, pure molten tin is reported to exhibit poor wetting of graphite at up to 1200 °C. The contact angles of high-purity (≥99.99%) tin liquid on dense (≤7% porosity) graphite in high-purity (99.999%) argon or reducing (5% H_2/Ar) atmospheres at 300–1200 °C have been reported to be ≥122 degrees (Weltsch et al., 2013; Sanchez et al., 2008). The contact angles reported for high-purity (≥99.99%) tin liquid on dense SiC in argon (> 99.9% purity, 1 atmosphere) or vacuum (10^{-8} atmospheres) at 800–1400 °C were ≥105 degrees (Liu et al., 2010; Tsoga et al., 1997; Takahashi and Kuboi, 1996; Nikolopoulos et al., 1992). These values were similar to measured contact angles of liquid tin on silica (Harding and Rossington, 1970), which was consistent with the presence of a silica scale on the silicon carbide surface. Non-wetting behavior (contact angles greater than 90°) has also been reported for molten tin at 600–1400 °C on mullite-based refractories (Ignatova et al., 1971). While this data indicates that pure liquid tin should not wet, or exhibit appreciable penetration into, porous graphite, silicon carbide, or mullite, the influence of impurities in various commercial grades of tin on such wetting/penetration at 1350 °C remains to be examined.

Regarding oxidation or reduction by reaction with an external gas environment, graphite and silicon carbide are stable in sufficiently reducing atmospheres, whereas mullite is stable in a sufficiently oxidizing atmosphere. At 1350 °C and 1 atm total pressure, graphite can coexist at equilibrium with an O_2-CO-CO_2 gas mixture possessing an oxygen partial pressure, p_{O2}, of 4.3×10^{-17} atm (Barin, 1995). At lower oxygen partial pressures (*i.e.*, higher p_{CO} and lower p_{CO2} values), graphite should not oxidize at 1350 °C and 1 atm. At 1350 °C and 1 atm, SiC can coexist with graphite and an O_2-SiO-CO-CO_2 gas mixture possessing a p_{O2} of 4.3×10^{-17} atm and a carbon dioxide partial pressure, p_{CO2}, of 2.4×10^{-4} atm (Barin, 1995). At lower partial pressures of

oxygen and carbon dioxide with graphite, SiC should be thermodynamically stable. At 1350 °C and 1 atm, mullite can coexist with alumina and a SiO(g)-rich gas mixture possessing a p_{O2} of 2.1×10^{-26} atm (Barin, 1995). At higher oxygen partial pressures (and lower partial pressures of SiO(g)), mullite should be thermodynamically stable at 1350 °C. (Details of these thermodynamic calculations are provided in Supplemental Information.)

In the absence of catalysts, the rate of oxidation of pure graphite of modest specific surface area ($< 3\ m^2/g$) in flowing dry air becomes appreciable above ~600 °C (Sampath et al., 1985; McKee, 1970; Heintz and Parker, 1966; Walker et al., 1959). In a dry atmosphere at oxygen partial pressures in excess of $\sim 10^{-3}$ atm at 1350 °C, SiC exhibits passive oxidation behavior, with the formation of a SiO_2 scale that thickens at a parabolic (decreasing) rate with time (Narushima et al., 1997; Jacobson, 1993). However, at lower oxygen partial pressures at 1350 °C, SiC can undergo more rapid active oxidation associated with the formation of SiO(g) (Jacobson and Myers, 2011). As mentioned above, mullite is thermodynamically stable in air at 1 atm up to the mullite incongruent melting temperature of 1890 °C (Klug et al., 1987; Horibe and Kuwabara, 1967).

Regarding thermal conductivity, the choice of graphite, silicon carbide, or mullite provides values spanning an order of magnitude at 1350 °C. Although the thermal conductivity of graphite is highly anisotropic (*i.e.*, two orders of magnitude higher along the graphite basal plane than perpendicular to the basal plane), use of the analysis of Pedraza and Klemens (1993) to estimate the effective conductivity of dense pyrolytic polycrystalline graphite from the measured basal plane conductivity of such graphite (Touloukian et al., 1970) yields a value of ~50 W/m K at 1350 °C. Interpolation of measured high-temperature thermal conductivity values of 96% dense polycrystalline silicon carbide (Touloukian et al., 1970; Fieldhouse et al., 1957) yields a value of ~21 W/m K at 1350 °C. Interpolation of measured high-temperature thermal conductivity values of dense, polycrystalline mullite at 1350 °C yields a value of ~4 W/m K (Hildmann and Schneider, 2005; Kingery et al., 1954).

Regarding thermal expansion, graphite, silicon carbide, and mullite provide a range of values. Values of the thermal expansion coefficient of graphite perpendicular to the c axis crystallographic direction (within the hexagonal planes) are quite small and range from about -1.4×10^{-6}/°C to 1.1×10^{-6}/°C from room temperature to 1350 °C, whereas the thermal expansion along a direction parallel to the c-axis is much larger with coefficients of $\sim 27 \times 10^{-6}$/°C to 29×10^{-6}/°C over this same temperature range (Kelly and Walker, 1970; Kellett and Richards, 1963; Martin and Entwisle, 1962). Hence, the thermal expansion of a graphite component along a given macroscopic direction will depend on the degree of grain alignment of the graphite crystals which, in turn, may be tailored with proper selection of the processing method used to generate the graphite component (*e.g.*, extrusion vs. isostatic compaction). The average linear thermal expansion coefficient for α-SiC is reported to be $\sim 4.6 \times 10^{-6}$/°C from room temperature to 1350 °C (Li and Bradt, 1986). The average linear thermal expansion coefficient for mullite is reported to be $5.3–5.6 \times 10^{-6}$/°C from 300 °C to 1000 °C (Brunauer et al., 2001; Schneider and Eberhard, 1990) and 7.5×10^{-6}/°C from 1000 °C to 1600 °C (Brunauer et al., 2001).

Regarding high-temperature stiffness and creep resistance, all three of these materials remain relatively rigid at elevated temperatures. The Young's modulus of isostatically-pressed (isotropic) sintered graphite (with a bulk density of 1.77–1.78 g/cm^3) increases from 8 to 10 GPa at room temperature to ~12–14 GPa at 1350 °C (Berto et al., 2015; Liu et al., 2015; Eto et al., 1991; Maruyama et al., 1987). The reported Young's moduli of polycrystalline, high-density silicon carbide and mullite are considerably higher, with values of ~332 GPa for α-SiC (with a bulk density of 2.98 g/cm^3) at 1350 °C (Fukuhara and Abe, 1993), 272 GPa for β-SiC (with a bulk density of 3.21 g/cm^3) at 1400 °C (Gulden, 1969), and ~213 GPa for mullite (with bulk density of 3.16 g/cm^3) at 1350 °C (Ledbetter et al., 1998). The creep of dense, isotropic polycrystalline graphite is negligible at ≤1350 °C (i.e., creep measurements for such graphite are typically conducted at ≥2000 °C; Narisawa et al., 1994; Green et al., 1970; Fischbach, 1960). The steady-state creep rate of dense (> 98%) fine-grained (2–5 μm) sintered α-SiC (such as Hexoloy SiC) at ≤1350 °C and ≤150 MPa is $\leq 10^{-10}$/sec (Lane et al., 1988; Wiederhorn et al., 1999). The reported steady-state creep rate of dense (> 95%) fine-grained (≤7 μm) mullite at ≤1300 °C and ≤50 MPa is $\leq 10^{-8}$/sec (Rhanim et al., 2003; Torrecillas et al., 1999). Along with attractive values of high-temperature stiffness and creep resistance (relative to conventional structural metal alloys), graphite, silicon carbide, and mullite are also brittle materials with modest values of fracture strength and fracture toughness (50 MPa and 1.1 MPa m$^{1/2}$ for 93% dense isostatic graphite, ≤500 MPa and ≤ 4.4 MPa m$^{1/2}$ for ≥95% dense sintered α-SiC, ≤500 MPa and ≤2.8 MPa m$^{1/2}$ for ≥95% dense mullite; Berto et al., 2015; Maruyama et al., 1987; Wiederhorn et al., 1999; Kim et al., 1998; Aksay et al., 1991; Ismail et al., 1987; Kanzaki et al., 1985). The brittle nature of these three stiff materials needs to be considered in the design of components (pipes, tanks, pumps *etc.*) for handling high-temperature tin liquid. For example, an external, room temperature (thermally insulated) metal infrastructure can be used to support such brittle materials, so as to minimize the tensile stresses (such as bending stresses) that would otherwise be experienced if these stiff materials were free-standing. Indeed, such a thermally-insulated, metal-backing strategy has recently been demonstrated in the design and successful testing of a ceramic/graphite-based pump used to control the flow of liquid tin at 1200–1400 °C (Amy et al., 2017). Thermally-insulated metallic structures may also be used to provide external support for graphite, silicon carbide, or mullite liners in pipes and tanks.

Regarding commercial availability, graphite, silicon carbide, and mullite have been used for many decades as refractory materials for high-temperature components (e.g., furnace/tank/tube linings, regenerators/heat exchangers, graphite/silicon carbide electrodes and heating elements, burners, *etc.*) in a number of large-scale materials manufacturing industries (e.g., steelmaking, aluminum smelting, glass manufacturing, cement manufacturing; Dana et al., 2014; Wang et al., 2012; Gianella et al., 2012; Yurkov, 2006; Klischat, 2005; Skurikhin and Ermakov, 2004) and, as a result, all three of these refractory materials are available in a variety of forms (tubes, crucibles, bricks, *etc.*) and sizes by a number of vendors. *Regarding relative costs*, comparisons of reported prices of shaped graphite, silicon carbide, and mullite components may be made to those of 316 stainless steel and Inconel 600 (high-temperature structural metal alloys) as reference points. For example, reported prices for graphite and mullite tubes ($38.4/foot and $51.6/foot, respectively, for 1 in. outer diameter (OD) × 0.75 inch inner diameter (ID) × 2.5–3 foot long tubes) and for sintered α-SiC tubes ($41.8/foot for 1 in. OD × 0.53 inch ID × 3 foot long tubes) fall between the reported prices of 316 stainless steel tubes and Inconel 600 tubes ($9/foot and $105/foot, respectively, for 1 inch OD × 0.83 ID × 6 foot long tubes) [MTI Corp., 2017; graphitestore.com, 2017; SentroTech, 2017; Grainger Industrial Supply, 2017; Wilk, 2016].

In summary, graphite, silicon carbide, and mullite may be attractive candidate containment materials for tin-based liquids at 1350 °C at 1 atm pressure owing to their thermal and mechanical stabilities (high melting or dissociation temperatures; retained stiffnesses and creep resistances at high temperatures), their anticipated resistances to infiltration and chemical attack by tin-based liquids of appropriate purity, and their commercial availabilities in different shapes. These candidate materials also provide ranges of thermal conductivities, thermal expansion coefficients, and resistances to oxidation or reduction (*i.e.*, required operational atmospheric environment) for use as components in the handling or containment of molten tin under varied conditions. However, the chemical interaction of these refractory materials with, or infiltration by, tin-bearing liquids of varied commercial purities at > 1300 °C and 1 atm pressure has not been examined. In the following sections of this paper, the reaction of various grades (purities) of

molten tin with, and penetration into, commercially-available graphite, silicon carbide, and mullite tubes at 1350 °C have been evaluated. Conditions under which chemical reaction(s) can be appreciably reduced or avoided have also been identified and demonstrated.

3. Experimental procedures

3.1. Starting materials

Commercial graphite, silicon carbide, and mullite tubes were exposed to tin-based liquids at 1350 °C. The graphite tubes (G347 grade, Graphite Products Corp., Madison Heights, MI) either possessed one closed end with an outer diameter (OD) of 1.0–1.2 cm and an inner diameter (ID) of 0.8 cm, or possessed open ends with OD/ID values of 1.5 cm/1.0 cm. The tube lengths were 5–10 cm. The graphite tubes possessed bulk densities of 1.74 ± 0.03 g/cm^3 (with corresponding bulk porosity values of 22.3 ± 1.4%, using a graphite theoretical density of 2.24 g/cm^3; ICDD, 2007) and purities (residual ash analyses) of ≥99.99%. The silicon carbide tubes (α-SiC, STS-100, SentroTech, Strongsville, OH) possessed OD/ID values of 2.5 cm/1.5 cm, lengths of 1.6–1.8 cm, bulk densities of 2.53 ± 0.06 g/cm^3 (with corresponding porosity values of 21.9 ± 1.9%, using an α-SiC theoretical density of 3.24 g/cm^3; ICDD, 2007), and elemental purities of ≥99.9%. X-ray diffraction (XRD) analyses yielded diffraction peaks for only the hexagonal polymorph of SiC. The mullite tubes (MV30, McDanel, Beaver Falls, PA) possessed OD/ID values of 1.26 cm/0.80 cm, 5 cm lengths, bulk densities of 2.51 ± 0.01 g/cm^3, and a purity of 97.9% (with Fe_2O_3/0.5%, TiO_2/0.5%, Na_2O + K_2O/0.8%, and MgO + CaO/0.3%). Quantitative XRD analyses (Rietveld whole pattern analyses by the vendor) indicated the presence of 9.4 wt% Al_2O_3 along with mullite. Using theoretical density values of 3.99 g/cm^3 for alumina and 3.17 g/cm^3 for mullite (ICDD, 2007), the mullite bulk density of 2.51 ± 0.01 g/cm^3 corresponded to a bulk porosity of 22.3 ± 0.3%.

Tin was purchased as shot (Alpha Aesar, Ward Hill, MA) with purities (metals basis) of 99%, 99.8%, 99.99%, and 99.999%. The major impurities (≥200 ppm levels) present in 99% and 99.8% purity tin were antimony, copper, and lead. The major impurities (at 0.4–2 ppm) in 99.99% and 99.999% purity tin were antimony, copper, and silver. Zinc granules (99.8% purity, with ≤100 ppm Fe, ≤100 ppm Pb; Alpha Aesar) were added to 99.8% purity tin to generate a 98 wt% Sn/2 wt% Zn composition (a synthetic "block tin" type liquid). Silicon additions (99.9999% purity, Alpha Aesar) were made to 99.8% purity tin to generate alloy liquids with 0.059 wt% (0.25 at.%), 0.12 wt% (0.50 at.%), or 0.24 wt% (1.0 at.%) silicon. The Sn-Zn and Sn-Si compositions were alloyed by melting in an alumina crucible (99.8% purity, CoorsTek, Golden, CO) at 1200 °C for 24 h within oxygen-gettered argon at 1 atm. Such oxygen gettering was conducted by passing ultra-high-purity argon (UHP 5.0, 99.999% purity, Airgas) over heated titanium within an oxygen-gettering system (Model OG-120 M, OXY-GON, Epsom, NH) to yield an oxygen partial pressure (p_{O2}) of 10^{-23} atm (measured with a zirconia-based oxygen sensor: CG-1000, Ametek, Pittsburgh, PA). After solidification, the resulting ingots were cut into smaller pieces and remelted at 1200 °C for an additional 24 h under the same conditions. The solidified ingots were again cut into smaller pieces and remelted for a third time under the same conditions, to allow for chemical homogenization. These low-Si alloys were evaluated by inductively-coupled plasma mass spectroscopy (ICP-MS, University of Georgia) and found to be comprised of 0.27 ± 0.02 at.%, 0.52 ± 0.03 at.%, and 0.94 ± 0.03 at.%, respectively (*i.e.*, close to the targeted values).

3.2. Molten tin exposure setup and conditions

Both-end-open graphite tubes were completely immersed in a given tin-based liquid as shown in Fig. 1. Because the density of liquid tin at 1350 °C (6.14 g/cm^3; Wang et al., 2003) is greater than the density of the graphite tube materials, horizontal graphite tube specimens were held below the surface of the tin-based liquid by two graphite rods fixed in position in the graphite container (Fig. 1a, b). For a given immersion trial, the graphite specimen-bearing container was loaded with sufficient tin-based liquid as to allow for complete immersion of the specimen. Bottom-end-closed graphite tube specimens were oriented vertically (Fig. 2) and partially filled with 6 g or 12 g (for 5 cm or 10 cm tall tubes, respectively) of a given tin-based composition, to achieve liquid tin columns at 1350 °C with heights of ~1.9 cm and ~4.0 cm, respectively. Both-end-open silicon carbide tubes were completely immersed in tin-based liquids in a similar manner as for the both-end-open graphite tubes. Both-end-open mullite tubes were completely immersed in tin-based liquid using two configurations shown in Fig. 3. For one configuration (Fig. 3a), the mullite tube sample was in direct contact with the graphite crucible and with the graphite rods used to hold the mullite tube below the liquid tin surface. For the second configuration (Fig. 3b), the mullite tube sample rested on a mullite plate and was held below the liquid tin surface by an alumina tube. The mullite tube-bearing containers were then loaded with sufficient tin to ensure complete immersion of the mullite tube sample at 1350 °C.

A graphite lid was used for all specimen configurations to minimize evaporative loss of tin at 1350 °C (the equilibrium tin vapor pressure at 1350 °C is 7.1 × 10^{-5} atm; Barin, 1995). The tube/tin-bearing assemblies were loaded into a controlled atmosphere horizontal tube furnace that was then sealed with stainless steel endcaps. After evacuation and backfilling several times with ultra-high-purity argon (UHP 5.0, 99.999% purity, Airgas USA, Marietta, GA), the argon entering the tube furnace was passed over heated titanium within an oxygen-gettering system until a measured p_{O2} of 10^{-23} atm was achieved (as discussed in the previous section). The tube furnace was then heated at 2 °C/min to 600 °C, and then at 1 °C/min to 1350 °C, followed by holding at 1350 °C for 100 h. After cooling, the lids were removed and the tube/tin-bearing assemblies were recovered.

3.3. Weight change measurements and microscopic analyses

A given tube/tin-bearing assembly was placed upside down over another graphite container within a controlled atmosphere vertical tube furnace that was then sealed with endcaps. After evacuation and backfilling with ultra-high-purity argon, and then flowing oxygen-gettered argon to achieve a measured p_{O2} of 10^{-23} atm, the tube/tin-bearing assembly was heated at 2 °C/min to 600 °C and held for 0.5 h to allow the tin-based solid to melt and drain into the underlying graphite container. After cooling, the weight of the recovered solidified tin in the bottom graphite container was measured to allow for comparison with the starting weight of tin placed in the assembly. Some of the recovered graphite, silicon carbide, and mullite tube specimens were placed in 12 N HCl for 2 h to selectively dissolve any solidified tin adhering to, or accessible within, the porous tube walls. Weights of the tin-free tubes were then measured to allow for comparison with starting tube weights. The resolution of the electronic microbalance used for such mass measurements was 1 × 10^{-4} g (0.1 mg).

Cross-sections of exposed graphite, silicon carbide, and mullite tube surfaces were also prepared for electron microscopic analyses. For these specimens, the bulk of the tin-based liquid was drained from the tube as described above. Any remaining solidified tin-based liquid on or within the tube surfaces was purposely retained (*i.e.*, these tube specimens were not exposed to the 12 N HCl etching treatment). The tubes were then filled with metallographic mounting epoxy. The epoxy-bearing tubes were cut with a wafering saw so as to capture the tin-liquid-exposed surfaces in the cross-sections. The graphite tube specimens were then ground to a thickness of ~100 μm, followed by dimpling and ion milling to perforation (to avoid smearing of the graphite across the epoxy/graphite interface). The mullite and silicon carbide tube specimens were polished using a series of diamond pastes to a surface finish of 1 μm.

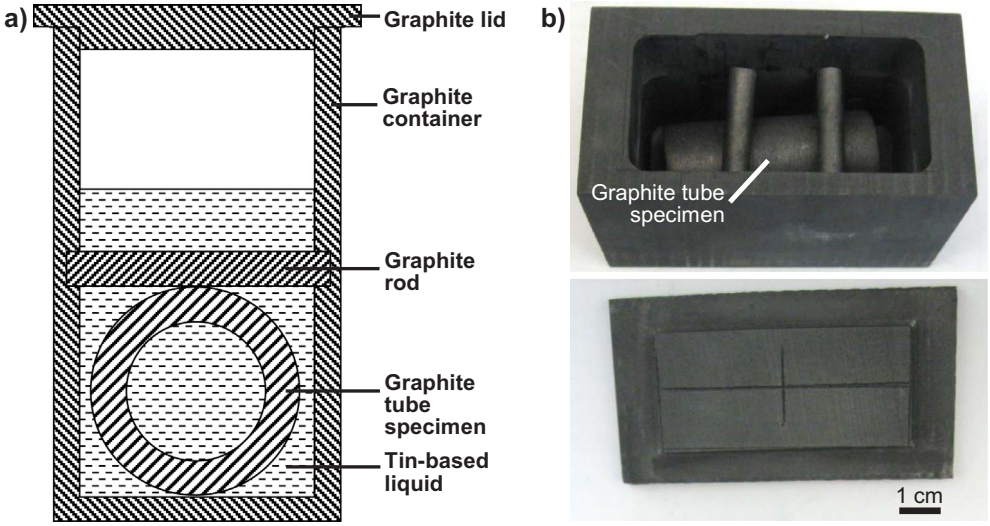

Fig. 1. (a) Schematic illustration (side view) of the test configuration for holding a horizontally-oriented graphite tube specimen under a tin-based liquid (using graphite rods) in a graphite container used for immersion studies for 100 h at 1350 °C. (b) Photographs (top-down view) of a horizontal graphite tube specimen held in place by two graphite rods in the graphite container (the graphite tube sample is outlined in a white rectangle) and of the graphite lid for the container.

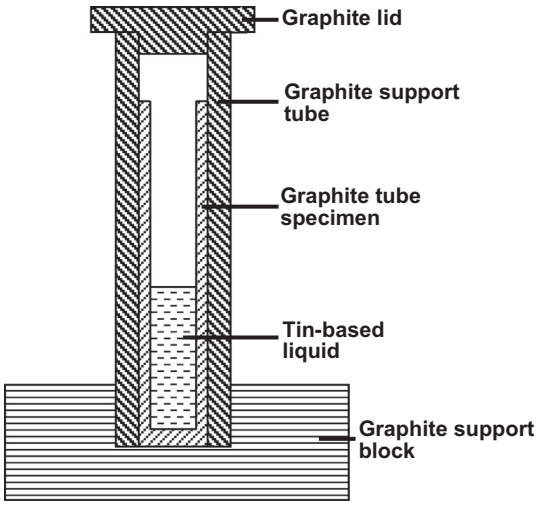

Fig. 2. Schematic illustration (side view) of the vertical test arrangement used to evaluate the extent of penetration of tin-based liquids into the porous walls of the graphite tube specimens at 1350 °C.

4. Results and discussion

4.1. Graphite interaction with liquid tin

Secondary electron images of ion-milled cross-sections of internal bottom surfaces of graphite tubes that had been exposed to the 98 wt% Sn/2 wt% Zn liquid or the 99.999 wt% Sn liquid for 100 h at 1350 °C are shown in Fig. 4. Similar images were obtained for graphite tubes exposed to the other tin-based liquids. The solidified tin-bearing phase was clearly detected as bright particles located at the surfaces of the graphite tubes. The spherical nature of these particles, and their presence only at external graphite surfaces, indicated that the 98–99.999% purity tin-based liquids did not wet the graphite tubes at 1350 °C, so that these liquids did not exhibit any appreciable penetration into the graphite tubes at this temperature. The penetration of tin-based liquids at 1350 °C into the graphite tubes was also assessed by measurements of the starting and recovered weights of the tin-based compositions (Table 1). Virtually all ($\geq$99.95%) of each type of the tin-based liquids was recovered from the graphite tubes, which was consistent with the observed lack of wetting (Fig. 4) and non-penetration of these tin-rich liquids into the porous graphite.

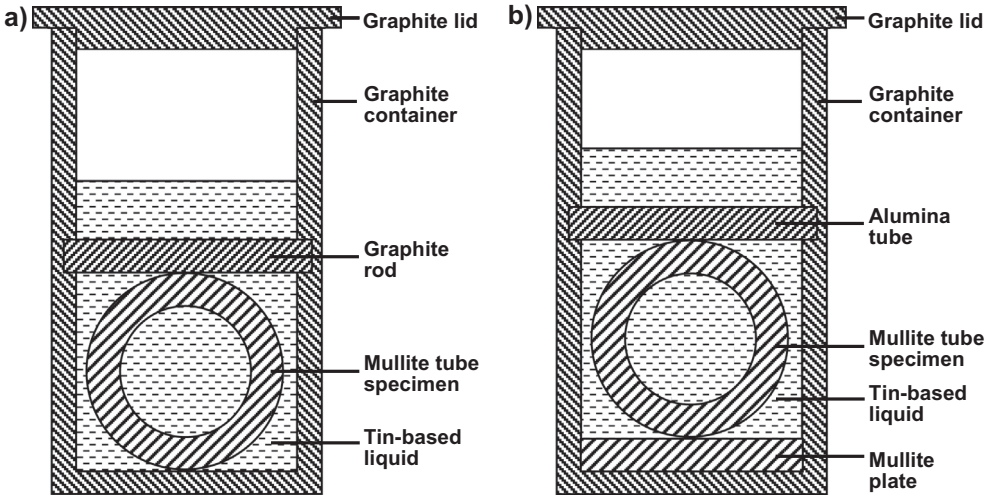

Fig. 3. Schematic illustrations (side views) of two test configurations for holding horizontally-oriented mullite tubes under a tin-based liquid for 100 h at 1350 °C. The mullite tube is in direct contact with graphite rods and the graphite container in the configuration shown in (a), whereas the mullite tube is physically isolated from graphite in the configuration shown in (b).

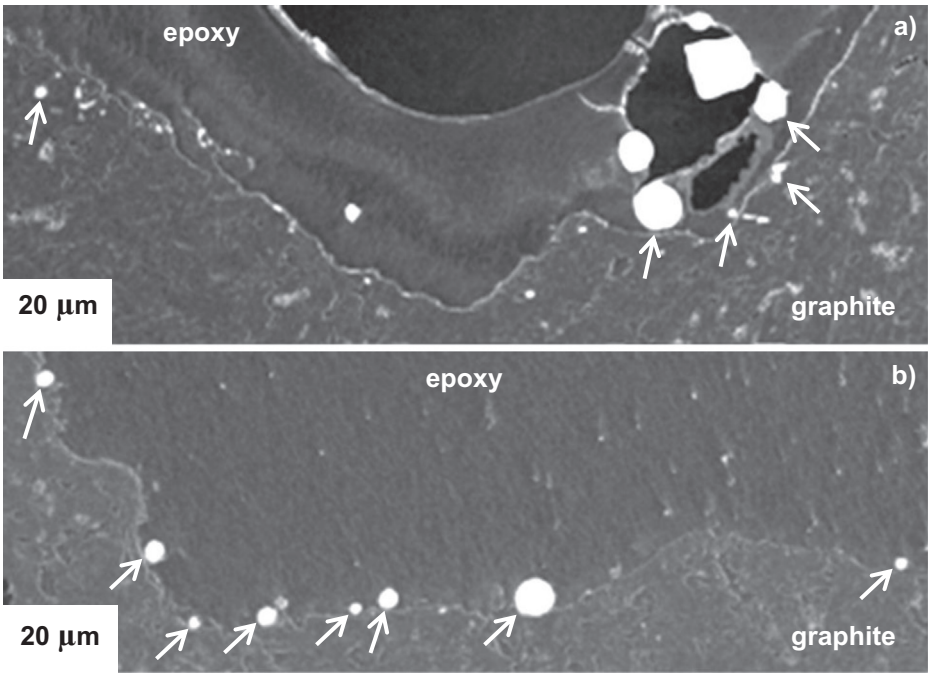

Fig. 4. Secondary electron images of cross-sections of graphite tubes obtained at graphite surfaces that had been exposed for 100 h at 1350 °C to: (a) 98 wt% tin liquid and (b) 99.999 wt% tin liquid. These cross-sections were obtained at the internal bottom surfaces of vertical, one-end-closed graphite tubes that had contained the tin-based liquids. Bright spherical tin-bearing particles are seen at the graphite surfaces (a number of these particles are identified with arrows).

Table 1
Evaluation of the recovery of tin-based liquids exposed to graphite tubes for 100 h at 1350 °C.

Graphite tube no. – orientation/type[a]	Tube dimensions (OD × ID × IL, mm)	Tin Purity (%)	Starting Tin Mass (g)	Tin Recovered (%)
1 – Vertical/OEC	12.0 × 8.0 × 46.1	98.0	6.4444	99.96
2 – Vertical/OEC	12.0 × 8.0 × 46.1	98.0	6.4528	99.95
3 – Vertical/OEC	10.0 × 8.0 × 95.8	98.0	12.1066	99.96
4 – Vertical/OEC	10.0 × 8.0 × 95.6	98.0	12.0403	99.96
5 – Vertical/OEC	12.0 × 8.0 × 46.0	99.0	5.9497	99.96
6 – Vertical/OEC	12.0 × 8.0 × 46.0	99.0	5.9674	99.96
7 – Vertical/OEC	12.0 × 8.0 × 46.1	99.8	6.0361	99.96
8 – Vertical/OEC	12.0 × 8.0 × 46.0	99.8	6.0304	99.96
9 – Vertical/OEC	10.0 × 8.0 × 95.6	99.8	12.0484	99.96
10 -Vertical/OEC	10.0 × 8.0 × 95.8	99.8	12.1058	99.96
11 – Horizontal/BEO	15.0 × 10.1 × 51.6	99.8	189.989	99.97
12 – Horizontal/BEO	15.0 × 10.1 × 52.9	99.8	190.894	99.98
13 – Vertical/OEC	12.0 × 8.0 × 46.0	99.99	5.9869	99.96
14 – Vertical/OEC	12.0 × 8.0 × 46.0	99.99	6.0296	99.95
15 – Horizontal/BEO	15.0 × 10.0 × 51.9	99.99	176.232	99.97
16 – Horizontal/BEO	15.0 × 10.0 × 51.5	99.99	176.112	99.97
17 – Vertical/OEC	12.0 × 8.0 × 46.0	99.999	5.9621	99.96
18 – Vertical/OEC	12.0 × 8.0 × 46.0	99.999	6.0125	99.96
19 – Vertical/OEC	10.0 × 8.0 × 95.8	99.999	12.0568	99.96
20 – Vertical/OEC	10.0 × 8.0 × 95.7	99.999	12.1033	99.96

[a] OEC = one end closed; BEO = both ends open.

Table 2
Evaluation of the weight loss per area and recession of graphite tubes exposed to tin-based liquids for 100 h at 1350 °C.

Graphite Tube no. – orientation/type[a]	Tin purity (%)	Starting graphite mass (g)	Graphite tube mass loss/area (g/cm^2)	Graphite recession (µm)[b]
1 – Vertical/OEC	98.0	5.7389	7.0×10^{-5}	0.40
2 – Vertical/OEC	98.0	5.6746	6.9×10^{-5}	0.41
3 – Vertical/OEC	98.0	5.5615	3.9×10^{-5}	0.22
4 – Vertical/OEC	98.0	5.5693	3.9×10^{-5}	0.22
5 – Vertical/OEC	99.0	5.7827	7.5×10^{-5}	0.43
6 – Vertical/OEC	99.0	5.7332	5.6×10^{-5}	0.32
7 – Vertical/OEC	99.8	5.6283	5.5×10^{-5}	0.32
8 – Vertical/OEC	99.8	5.7543	7.4×10^{-5}	0.43
9 – Vertical/OEC	99.8	5.5706	3.9×10^{-5}	0.22
10 – Vertical/OEC	99.8	5.6622	2.9×10^{-5}	0.16
11 – Horizontal/BEO	99.8	8.5355	7.1×10^{-6}	0.04
12 – Horizontal/BEO	99.8	8.7523	1.4×10^{-5}	0.08
13 – Vertical/OEC	99.99	5.7396	5.6×10^{-5}	0.32
14 – Vertical/OEC	99.99	5.7825	7.4×10^{-5}	0.42
15 – Horizontal/BEO	99.99	8.7032	7.0×10^{-6}	0.04
16 – Horizontal/BEO	99.99	8.6749	1.2×10^{-5}	0.07
17 – Vertical/OEC	99.999	5.7733	7.4×10^{-5}	0.43
18 – Vertical/OEC	99.999	5.6577	5.6×10^{-5}	0.32
19 – Vertical/OEC	99.999	5.5608	3.9×10^{-5}	0.22
20 – Vertical/OEC	99.999	5.6613	2.9×10^{-5}	0.16

[a] OEC = one end closed; BEO = both ends open.
[b] Calculated from the graphite weight lost, the bulk graphite tube density, and the exposed graphite surface area.

The effect of the purity of commercial tin on the graphite recession during exposure for 100 h at 1350 °C was also determined. The mass loss per area values of the graphite tubes after such exposure are shown in Table 2. For the vertical, one-end-closed graphite tubes, the weights of the tin-based compositions placed in the tubes (Table 1) were divided by 6.14 g/cm^3 (the density of liquid tin at 1350 °C; Wang et al., 2003) to obtain the liquid tin volumes in these tubes at 1350 °C. The liquid tin volumes were then divided by the cross-sectional areas of the columnar liquid tin inside the tubes to obtain the liquid tin heights. The liquid tin heights were, in turn, used to calculate the internal surface areas of the graphite tubes exposed to the liquid tin column. The volume of graphite lost for each tube was obtained by dividing the measured weight loss of the graphite tube by the measured bulk density of the starting tube. The graphite recession values were then obtained by dividing the lost graphite volume by the exposed graphite surface area. The calculated

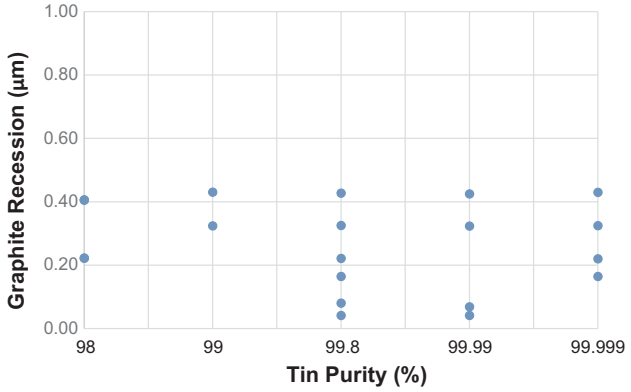

Fig. 5. Graphite recession after exposure to liquid tin of different purities for 100 h at 1350 °C.

graphite recession values are presented in Table 2 and Fig. 5. The graphite tubes exhibited very little mass loss per area ($\leq 7.5 \times 10^{-5}$ g/cm^2) with associated small calculated recession values (≤ 0.43 µm). No appreciable differences were detected in the graphite mass loss per area and graphite recession as a function of the tin purity.

4.2. Mullite interaction with liquid tin

Representative secondary electron images, and an associated elemental map, of a polished cross-section of an exposed surface of a both-end-open mullite tube that had been exposed to the 99.8 wt% tin liquid are shown in Fig. 6. As discussed above for the graphite cross-sections (Fig. 4), the spherical morphology and external surface location of residual solidified tin particles indicated a lack of wetting and penetration of the tin liquid into the mullite tube at 1350 °C. The starting weights of the tin batches exposed to the tubes, and the recovered tin weights (obtained after pouring tin out from the tubes) after the 1350 °C/100 h exposure are presented in Table 3. As can be seen from this table, virtually all of the tin liquid ($\geq$99.97%) was recovered, which was consistent with a lack of wetting and non-penetration of the tin liquid into the mullite tube (as well as the lack of wetting and non-penetration of the tin liquid into the G347 graphite crucibles and rods in contact with the tin and mullite tubes, consistent with the data in the previous section).

The changes in mass per area of the mullite tubes after exposure to the liquid tin for 100 h at 1350 °C were also evaluated (Table 3). The mass changes per area of the liquid-exposed mullite tubes that had been placed in direct contact with the graphite crucibles and rods (for the configuration shown in Fig. 3a) were 19–35 times higher than for the liquid-exposed mullite tubes that had not been placed in direct graphite

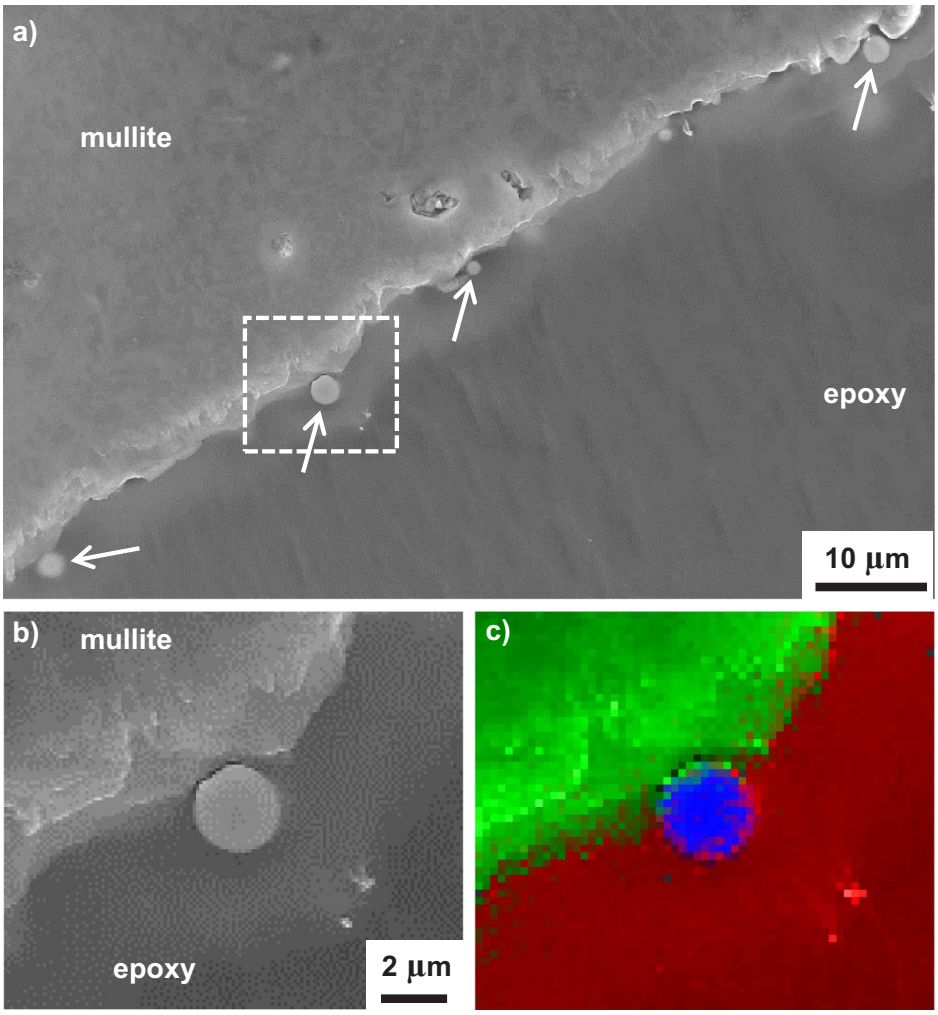

Fig. 6. (a) Secondary electron image of a cross section of a mullite tube sample obtained at a mullite surface that had been exposed for 100 h at 1350 °C to 99.8 wt% tin liquid. The arrows reveal spherical tin-bearing particles at the mullite surface. A higher magnification secondary electron image of the region shown in the white box is presented in (b), along with an associated elemental map obtained from energy-dispersive X-ray analysis (blue = tin, red = carbon, green = aluminum) in (c). (For interpretation of the references to colour in this figure legend, the reader is referred to the web version of this article.)

Table 3
Evaluation of the weight loss per area of, and tin penetration into, both-end-open mullite tubes fully immersed in tin liquid for 100 h at 1350 °C.

Mullite tube no.-support material	Tube dimensions (OD × ID × L, mm)	Starting tin mass (g)	Tin recovered (%)	Starting mullite mass (g)	Mullite tube mass loss/area (g/cm^2)	Mullite recession (μm)[a]
1-Graphite	12.6 × 8.0 × 50.8	180.863	99.97	9.4590	4.6×10^{-4}	1.8
2-Graphite	12.6 × 8.0 × 50.4	181.506	99.97	9.4100	5.9×10^{-4}	2.4
3-Alumina + Mullite	12.6 × 8.0 × 51.6	180.040	99.98	9.6046	1.7×10^{-5}	0.07
4-Alumina + Mullite	12.6 × 8.0 × 49.8	180.051	99.98	9.2581	2.4×10^{-5}	0.09

[a] Calculated from the mullite weight lost, the bulk mullite tube density, and the exposed mullite surface area.

contact (for the configuration shown in Fig. 3b). Mullite and carbon may undergo the following partial reduction reaction at elevated temperatures (Hong and Sahajwalla, 2013; Bentsen et al., 1985):

$$Al_6Si_2O_{13}(s) + 2C(s) = 3Al_2O_3(s) + 2SiO(g) + 2CO(g) \quad (3)$$

The excess solid carbon in the experimental setup could also react with the low-oxygen-bearing atmosphere in the horizontal tube furnace to yield CO(g) as follows:

$$C(s) + 1/2O_2(g) = CO(g) \quad (4)$$

The values of the standard Gibbs free energy changes of reactions (3) and (4) at 1350 °C and 1 atm pressure are +289,653 J/mol and −254,205 J/mol, respectively (Barin, 1995). Equilibration of solid carbon with an oxygen partial pressure of 10^{-23} atm by reaction (4) would yield a CO(g) partial pressure of 4.8×10^{-4} atm at 1350 °C. Equilibration of mullite, alumina, and carbon with this CO(g) partial pressure (via reaction (3)) at 1350 °C and 1 atm pressure would yield an equilibrium SiO(g) partial pressure of 4.6×10^{-2} atm (assuming ideal gas behavior for SiO(g) and CO(g), that $Al_6Si_2O_{13}$(s) and Al_2O_3(s) are present in their pure, stoichiometric reference states, and that C is present as pure graphite). Hence, if the local SiO(g) partial pressure at graphite/mullite interfaces dropped below this relatively high value of 4.6×10^{-2} atm at 1350 °C, then reaction (3) could occur. A control experiment was then conducted to determine whether mullite was being partially reduced by direct reaction with solid graphite. A mullite tube was placed in a graphite crucible and held in position using the configuration of Fig. 3a. This assembly (without tin) was then heated at 1350 °C for 100 h under the same flowing oxygen-gettered argon atmosphere. After the test, the mass loss of the mullite tube was measured to be 23.1 mg, which was similar to values obtained with the tin immersion experiments (15.7 mg, 20.3 mg). The mullite tube specimen was then cross-sectioned for electron microscopic analysis. A secondary electron image of such a cross-section, and an associated elemental map, are shown in Fig. 7. These images reveal a distinct alumina-rich reaction zone, with a thickness of about 60–80 μm, at the mullite surface that had been in direct contact with graphite. The alumina-enriched (silica-depleted) mullite surface observed in Fig. 7, and the similarity in mullite weight loss detected for this control (no liquid tin) experiment as for the liquid immersion experiments, indicated that the enhanced mullite mass loss was due to the direct reaction of mullite with solid graphite (as per reaction (3)) with negligible involvement of liquid tin. Such an alumina-enriched mullite surface was not detected for mullite tubes immersed in liquid tin for 100 h at 1350 °C using the configuration of Fig. 3b (*i.e.*, without direct contact of the mullite with solid graphite). The similar values of recovered tin (Table 3) for all of the liquid-immersed mullite tubes (with or without direct contact with graphite) were also consistent with the lack of tin involvement in such a mullite-graphite reaction process and, furthermore, indicated that liquid tin exhibited little global penetration into alumina-enriched mullite surfaces (generated by reaction with solid graphite) at 1350 °C.

4.3. Silicon carbide interaction with liquid tin

Representative secondary electron images, and an associated elemental map, of a polished cross-section of an exposed surface of a both-end-open α-SiC tube that had been exposed to the 99.8 wt% tin liquid are shown in Fig. 8. As discussed above for the graphite and mullite cross-sections (Figs. 4, 6), the spherical morphology and external surface location of residual solidified tin particles indicated a lack of wetting and penetration of the tin liquid into the α-SiC tube at 1350 °C. The recovered tin corresponded to 99.90% of the weight of the starting tin batch (285.349 g) exposed to α-SiC, which was consistent with negligible wetting and penetration into the α-SiC (and negligible penetration into the graphite crucible and graphite rods).

The changes in mass per area of the fully-immersed α-SiC tubes in the 99.8 wt% molten Sn and in the Sn-Si liquids are presented in Table 4. The mass changes per area of the α-SiC tubes exposed to 99.8 wt% molten tin (3.8×10^{-3} g/cm^2) were ≥90 times higher than for tubes exposed to the Sn-Si liquids. As has been reported for other carbide/liquid metal systems (Liu et al., 2009; Grzesik et al., 2003), silicon carbide may undergo an incongruent reaction of the following type with molten tin:

$$SiC(s) = \{Si\} + C(s) \quad (5)$$

where {Si} refers to silicon dissolved in molten tin. The standard Gibbs free energy change of reaction (5) at 1350 °C (for pure liquid silicon,

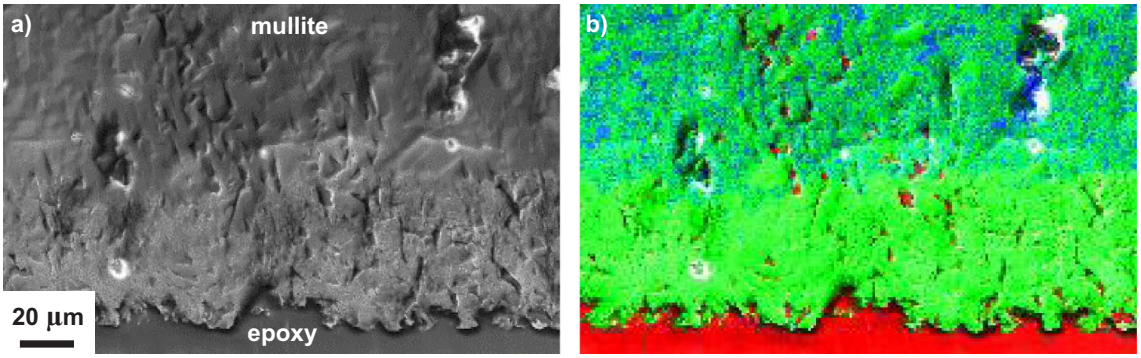

Fig. 7. (a) Secondary electron image and b) elemental mapping from energy-dispersive X-ray analysis (red = carbon; green = aluminum, blue = silicon) of a polished cross-section of a mullite tube sample (mounted in epoxy) that had been in direct contact with graphite at 1350 °C for 100 h in an oxygen-gettered argon atmosphere. (For interpretation of the references to colour in this figure legend, the reader is referred to the web version of this article.)

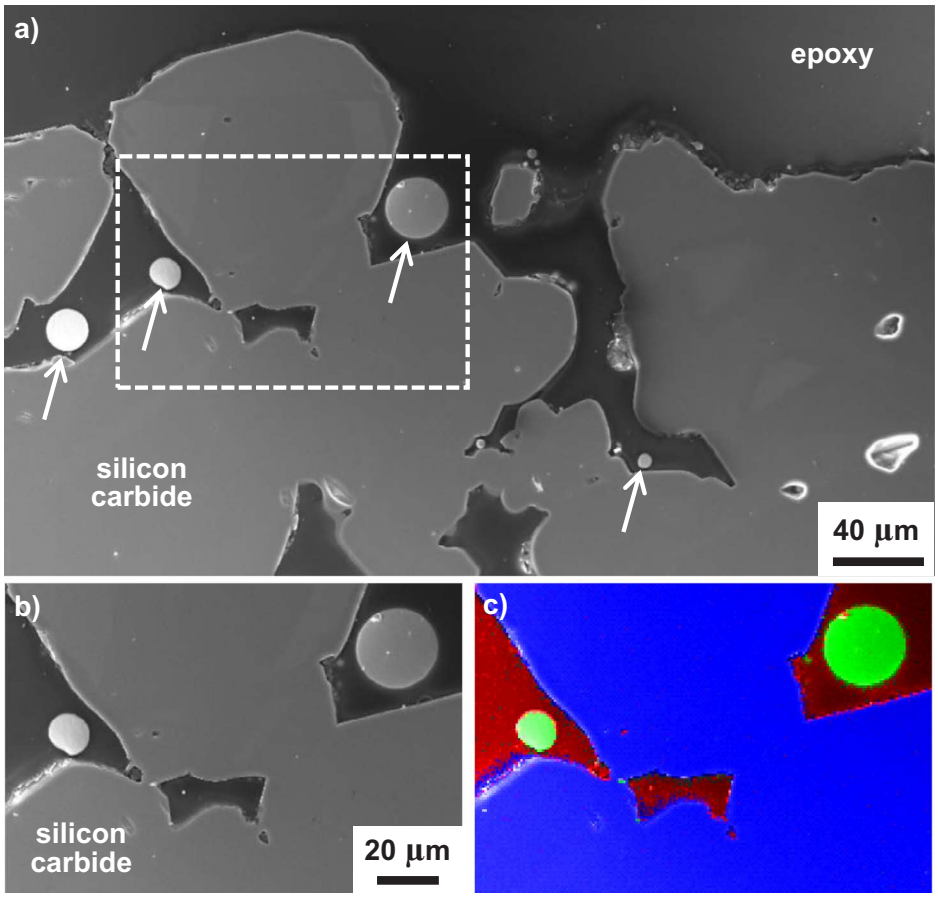

Fig. 8. (a) Secondary electron image of a cross section of a silicon carbide tube sample obtained at a silicon carbide surface that had been exposed for 100 h at 1350 °C to 99.8 wt% tin liquid. The arrows reveal spherical tin-bearing particles at the mullite surface. A higher magnification secondary electron image of the region shown in the white box is presented in (b), along with an associated elemental map obtained from energy-dispersive X-ray analysis (green = tin, red = carbon, blue = silicon) in (c). (For interpretation of the references to colour in this figure legend, the reader is referred to the web version of this article.)

pure solid graphite, and pure solid stoichiometric α-SiC reference states) is +59.7 kJ/mol (Barin, 1995; Pankratz et al., 1984). The silicon activity in molten tin associated with the equilibrium of reaction (5) at 1350 °C is 1.2×10^{-2}, which corresponds to an estimated Si atomic fraction of 1.6×10^{-3} or 0.16 at.% (using Si-Sn solution thermodynamic information from Heuzey and Pelton, 1996). As these thermodynamic calculations predicted, the addition of small amounts of silicon to the molten tin dramatically reduced (by factors of > 90 times) the mass loss per area of α-SiC during liquid immersion at 1350 °C (Table 4). Indeed, for tin melts containing ≥0.52 at.% silicon, the measured weight loss of silicon carbide was near or below the microbalance resolution (0.1 mg). While such modest silicon additions to tin will increase the liquidus temperature (*e.g.*, to 791 °C for a 0.65 at.% silicon addition to tin; Olesinski and Abbaschian, 1984a), the small amounts of solid silicon that would precipitate in such tin-based liquids below the liquidus temperature would not be expected to appreciably alter the properties of the tin-based liquid (*e.g.*, a 0.5 at.% silicon/99.5 at.% tin composition would correspond to a mixture of only 0.36 vol% solid silicon in 99.64 vol% liquid tin at just above the melting point of pure tin, 231.9 °C).

5. Summary

Raising the turbine operating temperature for CSP could significantly increase cycle efficiency (*e.g.*, to ~60% for turbine inlet temperatures > 1300 °C) with an associated dramatic reduction in the cost of generated electricity, if all other costs remain fixed. Molten tin is an attractive candidate heat transfer fluid for such high-temperature operation due to its high temperature chemical stability, low melting/high boiling points, high thermal conductivity, and low viscosity. However, high-temperature molten tin is quite corrosive to structural Fe-based and Ni-based alloys. Graphite, silicon carbide, and mullite are potential high-temperature materials for the containment of high-temperature molten tin. The penetration of molten tin into, and reaction of

Table 4
Evaluation of the weight loss per area of both-end-open silicon carbide tubes fully immersed in tin-based liquids for 100 h at 1350 °C.

Silicon carbide tube no.	Tube dimensions (OD × ID × L, mm)	Silicon content of the Tin (at.%)	Starting silicon carbide mass (g)	Silicon carbide tube mass loss/area (g/cm^2)	Silicon carbide recession (µm)[b]
1	25.0 × 14.6 × 16.8	0	13.4290	3.8×10^{-3}	15
2	25.0 × 14.7 × 17.2	0	13.7268	3.8×10^{-3}	15
3	24.9 × 14.9 × 17.9	0.27 ± 0.02	14.0370	4.2×10^{-5}	0.17
4	25.0 × 15.0 × 15.9	0.27 ± 0.02	12.5859	3.1×10^{-5}	0.12
5	24.9 × 14.9 × 17.1	0.52 ± 0.03	13.7144	7.3×10^{-6}	0.03
6	25.0 × 15.0 × 16.0	0.52 ± 0.03	12.8193	Not detectable[a]	–
7	24.9 × 14.9 × 17.7	0.94 ± 0.03	13.9915	Not detectable[a]	–
8	24.9 × 14.8 × 16.9	0.94 ± 0.03	13.4142	3.7×10^{-6}	0.01

[a] Not detectable within the resolution of the electronic balance (< 0.1 mg weight change).
[b] Calculated from the silicon carbide weight lost, the bulk silicon carbide tube density, and the exposed silicon carbide surface area.

molten tin with, commercially-available tubes of graphite, mullite, and silicon carbide have been examined after exposure of these tubes to tin-based liquids for 100 h at 1350 °C in a low-oxygen-bearing argon atmosphere. Local electron microscopic analyses of tube cross-sections, and global measurements of the weight of recovered tin from the tubes, indicated that molten tin did not wet and did not appreciably penetrate these tube materials during such 1350 °C/100 h exposure. Graphite exhibited little weight change ($\leq 7.5 \times 10^{-5}$ g/cm^2) and recession (≤ 0.4 μm) in molten tin of a variety of purities (98–99.999%) at 1350 °C. However, α-SiC exhibited significantly greater mass loss per area (3.8×10^{-3} g/cm^2) upon exposure to molten tin (99.8 wt% purity). The addition of small amounts (0.06–0.12 wt%) of soluble silicon to the tin liquid at 1350 °C dramatically reduced such SiC mass loss (to $\leq 4.2 \times 10^{-5}$ g/cm^2), which was consistent with a reduction in the incongruent dissolution of α-SiC in such liquids. Without direct contact to graphite, mullite also exhibited little mass loss per area ($\leq 2.4 \times 10^{-5}$ g/cm^2) in molten tin at 1350 °C. Direct contact of mullite with graphite at 1350 °C resulted in partial silica reduction (alumina enrichment) of the mullite, although with no appreciable effect on tin penetration into the mullite. Such silica reduction was avoided by physical separation of the mullite from graphite. Hence, under appropriate conditions, graphite, silicon carbide, and mullite can be compatible materials for the containment of tin-based liquids at 1350 °C in CSP systems.

Acknowledgements

This work supported by ARPA-E cooperative agreement number DE-AR0000339. The work of SH was supported by the U.S. Department of Energy via grant number DE-SC0014034. The manuscript preparation and editing work of KHS was supported by the U.S. Department of Energy via award number DE-EE0007117.

Appendix A. Supplementary material

Supplementary data associated with this article can be found, in the online version, at http://dx.doi.org/10.1016/j.solener.2018.01.085.

References

Aksay, I.A., Dabbs, D.M., Sarikaya, M., 1991. Mullite for structural, electronic, and optical applications. J. Am. Ceram. Soc. 74, 2343–2358.
Amy, C., Budenstein, D., Bagepalli, M., England, D., DeAngelis, A., Wilk, G., Jarrett, C., Kelsall, C., Hirschey, J., Wen, H., Chavan, A., Gilleland, B., Yuan, C., Chueh, W., Sandhage, K.H., Kawajiri, Y., Henry, A., 2017. Pumping liquid metal at high temperatures up to 1,673 K. Nature 550 (7675), 199–203.
Barin, I., 1995. Thermochemical Data of Pure Substances, third ed. VCH Verlagsgesellschaft mbH, Weinheim, Germany.
Bentsen, S., Joergensen, S., Wiik, K., Motzfeldt, K., 1985. Reactions between carbon and the oxides mullite and silica. Mater. Sci. Monogr. 28A, 621–626.
Berto, F., Campagnolo, A., Gallo, P., 2015. Brittle failure of graphite weakened by V-notches: a review of some recent results under different loading modes. Strength Mater. 47, 488–506.
Brooks, F.J., 2000. GE gas turbine performance characteristics. Report No. GER-3567H, GE Power Systems, Schenectady, NY. < http://ncad.net/Advo/CinerNo/ge6581b.pdf > .
Brunauer, G., Frey, F., Boysen, H., Scnheider, H., 2001. High temperature thermal expansion of mullite: an in-situ neutron diffraction study up to 1600 °C. J. Eur. Ceram. Soc. 21, 2563–2567.
Dana, K., Sinhamahapatra, S., Tripathi, H.S., Ghosh, A., 2014. Refractories of alumina-silica system. Trans. Ind. Ceram. Soc. 73, 1–13.
Dunn, B., Kamath, H., Tarascon, J.-M., 2011. Electrical energy storage for the grid: a battery of choices. Science 334, 928–935.
Dybkov, V.I., 1990. Interaction of 18Cr-10Ni stainless steel with liquid aluminum. J. Mater. Sci. 25, 3615–3633.
Elkin, B., Finkelstein, L., Dyer, T., Raade, J., 2014. Molten oxide glass materials for thermal energy storage. Energy Proc. 49, 772–779.
Emmerich, T., Schroer, C., 2017. Corrosion in austenitic steels and nickel-based alloys caused by liquid tin at high temperature. Corr. Sci. Ahead of Print.
Eto, M., Oku, T., Konishi, T., 1991. High temperature Young's modulus of a fine-grained nuclear graphite oxidized or prestressed to various levels. Carbon 29, 11–21.
Fieldhouse, I.B., Hedge, J.C., Lang. J.I., Waterman, T.E., 1957. Thermal properties of high-temperature materials. Report No. WADC-TR-57-487; AD-150954. Illinois Institute of Technology, Chicago, IL.
Fischbach, D.B., 1960. High-temperature creep of graphite. Nature 4727, 795–797.
Forsberg, C.W., Peterson, P.F., Zhao, H., 2006. High-temperature liquid-fluoride-salt closed-Brayton-cycle solar power towers. J. Solar Energy Eng. 129, 141–146.
Fukuhara, M., Abe, Y., 1993. High-temperature elastic moduli and internal frictions of α-SiC ceramic. J. Mater. Sci. 12, 681–683.
Ghoshal, U., Grimm, D., Ibrani, S., Johnston, C., Miner, A., 2005. High-performance liquid metal cooling loops. In: Proceedings of the Twenty First IEEE Semiconductor Thermal Measurement and Management Symposium, March 15, 2005, San Jose, CA, IEEE, Piscataway, NJ.
Gianella, S., Gaia, D., Ortona, A., 2012. High temperature applications of Si-SiC cellular ceramics. Adv. Eng. Mater. 14, 1074–1081.
Goyer, R.A., 1990. Lead toxicity: from overt to subclinical to subtle health effects. Environ. Health Perspect. 86, 177.
Grainger Industrial Supply, 2017. < https://www.grainger.com/category/stainless-steel-tubing/tubing/pipe-tubing-and-fittings/plumbing/ecatalog/N-qxd?okey=stainless+steel+tubing&mkey=Stainless+Steel+Tubing+&refineSearchString=stainless+steel+tubing&NLSCM=5&EndecaKeyword=stainless+steel+tubing&searchRedirect=stainless+steel+tubing&sst=subset&suggestConfigId=6 > .
graphitestore, 2017. < http://graphitestore.com/ > .
Green, W.V., Weertman, J., Zukas, E.G., 1970. High-temperature creep of polycrystalline graphite. Mater. Sci. Eng. 6, 199–211.
Grzesik, Z., Dickerson, M.B., Sandhage, K.H., 2003. The incongruent reduction of tungsten carbide by a zirconium-copper melt. J. Mater. Res. 18, 2135–2140.
Gulden, T.D., 1969. Mechanical properties of polycrystalline β-SiC. J. Am. Ceram. Soc. 52, 585–590.
Harding, P.L., Rossington, D.R., 1970. Wetting of ceramic oxides by molten metals under ultrahigh vacuum. J. Am. Ceram. Soc. 53, 87–90.
Heinzel, A., Weisenburger, A., Muller, G., 2017. Corrosion behavior of austenitic steel AISI 316L in liquid tin in the temperature range 280 and 700 °C. Mater. Corr., Ahead of Print.
Henry, A., Prasher, R., 2014. The prospect of high temperature solid state energy conversion to reduce the cost of concentrated solar power. Energy Environ. Sci. 7, 1819–1828.
Hernández-Moro, J., Martínez-Duart, J.M., 2013. Analytical model for solar PV and CSP electricity costs: present LCOE values and their future evolution. Renew. Sustain. Energy Rev. 20, 119–132.
Heuzey, M.-C., Pelton, A.D., 1996. Critical evaluation and optimization of the thermodynamic properties of liquid tin solutions. Metall. Mater. Trans. B 27B, 810–828.
Heintz, E.A., Parker, W.E., 1966. Catalytic effect of major impurities on graphite oxidation. Carbon 4, 473–482.
Hildmann, B., Schneider, H., 2005. Thermal conductivity of 2/1 mullite single crystals. J. Am. Ceram. Soc. 88, 2879–2882.
Hong, L., Sahajwalla, V., 2013. Metall. Mater. Trans. B 44, 1541–1545.
Horibe, T., Kuwabara, S., 1967. Thermo-analytical investigation of phase equilibria in the Al_2O_3-SiO_2 system. Bull. Chem. Soc. Jpn. 40, 972–982.
Huck, P., Freund, S., Lehar, M., Peter, M., 2016. Performance comparison of supercritical CO2 versus steam bottoming cycles for gas turbine combined cycle applications. In: Proc. 5th Int. Symp. Supercritical CO_2 Power Cycles. San Antonio, TX. < http://sco2symposium.com/4org/d18/sCO2/papers2016/SystemConcepts/092paper.pdf > . pp. 1–14.
ICDD (International Center for Diffraction Data), 2007. Newtown Square, PA USA. Card No. 41–1487 for graphite, Card No. 29–1131 for alpha silicon carbide, Card No. 10–0173 for alumina, Card No. 15–776 for mullite.
Ignatova, T.S., Nazarova, T.I., Buldakov, A.A., 1971. Wetting refractory materials with tin. Fiz. Khim. Poverkh. Yavlenii Vys. Temp. 162–165.
Ismail, M. G. M. U., Nakai, Z., Somiya, S., 1987. Microstructure and mechanical properties of mullite prepared by the sol-gel method. J. Am. Ceram. Soc. 70, C-7–C-8.
Jacobson, N.S., 1993. Corrosion of silicon-based ceramics in combustion environments. J. Am. Ceram. Soc. 76, 3–28.
Jacobson, N.S., Myers, D.L., 2011. Active oxidation of SiC. Oxid. Met. 75, 1–25.
Joseph, M., Sivakumar, N., Manoravi, P., 2002. High temperature vapor pressure studies on graphite using laser pulse heating. Carbon 40, 2021–2040.
Kanzaki, S., Tabata, H., Kumazawa, T., Ohta, S., 1985. Sintering and mechanical properties of stoichiometric mullite. J. Am. Ceram. Soc. 68, C-6–C-7.
Kellett, E.A., Richards, B.P., 1963. The thermal expansion of graphiate within the layer planes. J. Nucl. Mater. 12, 184–192.
Kelly, B.T., Walker Jr., P.L., 1970. Theory of thermal expansion of a graphite crystal in the semi-continuum model. Carbon 8, 211–226.
Kim, Y.-W., Mitomo, M., Emoto, H., Lee, J.-G., 1998. Effect of initial α-phase content on microstructure and mechanical properties of sinteted silicon carbide. J. Am. Ceram. Soc. 81, 3136–3140.
Kingery, W.D., Francl, J., Coble, R.L., Vasilos, T., 1954. Thermal conductivity: X, Data for several pure oxide materials corrected to zero porosity. J. Am. Ceram. Soc. 37, 107–110.
Kleykamp, H., Schumacher, G., 1993. The constitution of the silicon-carbon system. Ber. Bunsenges. Phys. Chem. 97, 799–805.
Klischat, H.-J., 2005. Refractory lining review for cement kiln systems. ZKG Int. 58, 33–45.
Klug, F.J., Prochazka, S., Doremus, R.H., 1987. Alumina-silica phase diagram in the mullite region. J. Am. Ceram. Soc. 70, 750–759.
Kolb, G.J., Ho, C.K., Mansini, T.R., Gary, J.A., 2011. Power tower technology roadmap and cost reduction plan. Sandia Report No. SAND2011-2419, Sandia National Laboratories, Albuquerque, NM.
Kumar, P., Dregia, S.A., Sandhage, K.H., 1999. Epitaxial growth of magnesia and spinel on sapphire during incongruent reduction in molten magnesium. J. Mater. Res. 14,

3312–3318.
Lane, J.E., Carter, C.H., Davis, R.F., 1988. Kinetics and mechanisms of high-temperature creep in silicon carbide: III, Sintered α-silicon carbide. J. Am. Ceram. Soc. 71, 281–295.
Ledbetter, H., Kim, S., Balzar, D., Crudele, S., Kriven, W., 1998. Elastic properties of mullite. J. Am. Ceram. Soc. 81, 1025–1028.
Leider, H.R., Krikorian, O.H., Young, D.A., 1973. Thermodynamic properties of carbon up to the critical point. Carbon 11, 555–563.
Li, Z., Bradt, R.C., 1986. Thermal expansion of the cubic (3C) polytype of silicon carbide. J. Mater. Sci. 21, 4366–4368.
Liu, G.W., Muolo, M.L., Valenza, F., Passerone, A., 2010. Survey on wetting of SiC by molten metals. Ceram. Int. 36, 1177–1188.
Liu, Y., Lipke, D.W., Zhang, Y., Sandhage, K.H., 2009. The kinetics of incongruent reduction of tungsten carbide (WC) via reaction with a hafnium-copper (Hf-Cu) melt. Acta Mater. 57, 3924–3931.
Liu, Z., Bao, Y.W., Wan, D.T., Tian, Y., Hu, C.L., Wei, C.G., 2015. A novel method to evaluate Young's modulus of ceramics at high temperature up to 2100°C. Ceram. Int. 41, 12835–12840.
Margolis, R., Coggeshall, C., Zuboy, J., 2012. SunShot vision study. U.S. Dept. of Energy, National Renewable Energy Laboratory. < https://energy.gov/sites/prod/files/2014/01/f7/ 47927.pdf > .
Martin, W.H., Entwisle, F., 1962. Thermal expansion of graphite over different temperature ranges. J. Nucl. Mater. 10, 1–7.
Maruyama, T., Eto, M., Oku, T., 1987. Elastic moduli and bend strength of a nuclear graphite at high temperature. Carbon 25, 723–726.
McKee, D.W., 1970. The copper-catalyzed oxidation of graphite. Carbon 8, 131–139.
Mehos, M., Turchi, C., Jorgenson, J., Denholm, P., Ho, C., Armijo, K., 2016. On the path to SunShot: Advancing concentrating solar power technology, performance, and dispatchability. Golden, CO: National Renewable Energy Laboratory. NREL/TP-5500-65688. < http://www.nrel.gov/docs/fy16osti/65688.pdf > .
Misra, A.K., Whittenberger, J.D., 1987. Fluoride salts and container materials for thermal energy storage applications in the temperature range 973 to 1400 K. NASA Technical Memorandum 89913. National Aeronautics and Space Administration, Lewis Research Center., Cleveland, OH (USA). < https://ntrs.nasa.gov/archive/nasa/casi.ntrs.nasa.gov/19870014593.pdf > .
MTI Corporation, 2017. < http://www.mtixtl.com/mullitetubes.aspx > .
Narisawa, M., Adachi, M., Souma, I., 1994. High-temperature creep and resultant anisotropy in ultrasonic velocity in isotropic graphite. J. Mater. Sci. 29, 708–713.
Narushima, T., Goto, T., Hirai, T., Iguchi, Y., 1997. High-temperature oxidation of silicon carbide and silicon nitride. Mater. Trans., JIM. 38, 821–835.
Nikolopoulos, P., Agathopoulos, S., Angelopoulos, G.N., Naoumidis, A., Grubmeier, H., 1992. Wettability and interfacial energies in SiC-liquid metal systems. J. Mater. Sci. 27, 139–145.
Oden, L.L., Gokcen, N.A., 1993. Sn-C and Al-Sn-C phase diagrams and thermodynamic properties of C in the alloys: 1550 °C to 2300 °C. Metall. Trans. B 24B, 53–58.
Olesinski, R.W., Abbaschian, G.J., 1984a. The Si-Sn (Silicon-Tin) system. Bull. Alloy Phase Diagr. 5, 273–276.
Olesinski, R.W., Abbaschian, G.J., 1984b. The C-Si (carbon-silicon) system. Bull. Alloy Phase Diagr. 5, 486–489.
Pacio, J., Fritsch, A., Singer, C., Uhlig, R., 2014. Liquid metals as efficient coolants for high-intensity point-focus receivers: implications to the design and performance of next-generation CSP Systems. Energy Proc. 49, 647–655.
Pacio, J., Wetzel, T., 2013. Assessment of liquid metal technology status and research paths for their use as efficient heat transfer fluids in solar central receiver systems. Sol Energy 93, 11–22.
Pankratz, L.B., Stuve, J.M., Gokcen, N.A., 1984. Thermodynamic Data for Mineral Technology. Bulletin 677. U.S. Department of the Interior, Bureau of Mines, Washington, DC, p. 136.
Pedraza, D.F., Klemens, P.G., 1993. Effective conductivity of polycrystalline graphite. Carbon 31, 951–956.
Pietzka, M.A., Schuster, J.C., 1997. Phase equilibria of the quaternary system Ti-Al-Sn-N at 900°C. J. Alloys Compounds 247, 198–201.
Rastler, D., 2010. Electricity energy storage technology options: a white paper primer on applications, costs and benefits. Technical Update Report No. 1020676. Electric Power Research Institute, Palo Alto, CA. < http://large.stanford.edu/courses/2012/ph240/doshay1/docs/EPRI.pdf > .
Reed, E.L., 1954. Stability of refractories in liquid metals. J. Am. Ceram. Soc. 37, 146–153.
Regel, A.R., Smirnov, I.A., Shadrichev, E.V., 1971. Thermal conductivity of salt, metal, and semiconducting melts. Phys. Stat. Sol. (a) 5, 13–57.
Rhanim, H., Olagnon, C., Fantozzi, G., Azim, A., 2003. High-temperature deformation of mullite and analysis of creep curves. J. Mater. Res. 18, 1771–1776.
Sampath, S., Kulkarni, N.K., Chackraburtty, D.M., 1985. Thermochim. Acta 86, 7–15.
Sanchez, S.A., Narciso, J., Louis, E., Rodriguez-Reinoso, F., Saiz, E., Tomsia, A., 2008. Wetting and capillarity in the Sn/graphite system. Mater. Sci. Eng. A 495, 187–191.
Sandhage, K.H., Yurek, G.J., 1991. Indirect dissolution of (Al, Cr)2O3 in CaO-MgO-Al2O3-SiO2 melts. J. Am. Ceram. Soc. 74, 1941–1954.
Sandhage, K.H., Yurek, G.J., 1990a. Direct and indirect dissolution of sapphire in CaO-MgO-Al_2O_3-SiO_2 melts: dissolution kinetics. J. Am. Ceram. Soc. 73, 3633–3642.
Sandhage, K.H., Yurek, G.J., 1990b. Indirect dissolution of sapphire into calcia-magnesia-alumina-silica melts: electron microprobe analysis of the dissolution process. J. Am. Ceram. Soc. 73, 3643–3649.
Sandhage, K.H., Yurek, G.J., 1988. Indirect dissolution of sapphire into silicate melts. J. Am. Ceram. Soc. 71, 478–489.
Scace, R.J., Slack, G.A., 1959. Solubility of carbon in silicon and germanium. J. Chem. Phys. 30, 1551–1555.
Schneider, H., Eberhard, E., 1990. Thermal expansion of mullite. J. Am. Ceram. Soc. 73, 2073–2076.
SentroTech, 2017. < http://www.sentrotech.com/ceramic-tubes/silicon-carbide/ > .
Skurikhin, V.V., Ermakov, I.N., 2004. Refractories for glass production. Glass Ceram. 61, 346–351.
Sobolev, V., 2010. Database of thermophysical properties of liquid metal coolants for GEN-IV. SCK-CEN, Scientific Report BLG-1069.
Sobolev, V., 2012. Properties of liquid metal coolants. Compr. Nucl. Mater. 2, 373–392.
Takahashi, S., Kuboi, O., 1996. Study on contact angles of Au, Ag, Cu, Sn, Al, and Al alloys to SiC. J. Mater. Sci. 31, 1797–1802.
Torrecillas, R., Calderon, J.M., Moya, J.S., Reece, M.J., Davies, C.K.L., Olagnon, C., Fantozzi, G., 1999. Suitability of mullite for high temperature applications. J. Eur. Ceram. Soc. 19, 2519–2527.
Touloukian, Y.S., Powell, R.W., Ho, C.Y., Klemens, P.G., 1970. Thermal conductivity of nonmetallic solids. Thermophysical Properties of Matter. vol. 2. IFI/Plenum. New York, NY. pp. 41, 585–588.
Tsoga, A., Ladas, S., Nikolopoulos, P., 1997. Correlation between the oxidation state of α-SiC and its wettability with non-reactive (Sn) or reactive (Ni) metallic components and their binary Si-alloys. Acta Mater. 45, 3515–3525.
U.S. Energy Administration Information, 2015. Levelized cost and levelized avoided cost of new generation resources in the annual energy outlook 2015. < https://www.eia.gov/outlooks/archive/aeo15/pdf/electricity_generation_2015.pdf > .
Walker, P.L., Rusinko Jr., F., Austin, L.G., 1959. Gas reactions of carbon. Adv. Catal. 11, 133–221.
Wang, Y., Bai, F., Jian, Y., Xu, C., Wang, Z., 2012. Heat transfer enhancement of an electric air heating furnace by inserting silicon carbide ceramic foam panels. Exp. Thermal Fluid Sci. 38, 127–133.
Wang, L., Wang, Q., Xian, A., Lu, K., 2003. Precise measurement of the densities of liquid Bi, Sn, Pb, and Sb. J. Phys. Condens. Matter 15, 777–783.
Weltsch, Z., Lovas, A., Takacs, J., Cziraki, A., Toth, A., Kaptay, G., 2013. Measurement and modelling of the wettability of graphite by a silver-tin (Ag-Sn) liquid alloy. Appl. Surf. Sci. 268, 52–60.
Wiederhorn, S.M., Hockey, B.J., French, J.D., 1999. Mechanisms of deformation of silicon nitride and silicon carbide at high temperatures. J. Eur. Ceram. Soc. 19, 2273–2284.
Wilk, G.C., 2016. Liquid Metal-based High Temperature Concentrated Solar Power: Cost Considerations. M.S. Thesis, Georgia Institute of Technology.
Yurkov, A.A., 2006. Refractories and carbon cathode materials for the aluminum industry. Refr. Ind. Ceram. 47, 139–145.